Lithium bis(oxalato)borate as an electrolyte for micromesoporous carbide-derived carbon based supercapacitors

ARTICLE *in* JOURNAL OF ELECTROANALYTICAL CHEMISTRY · MARCH 2012

Impact Factor: 2.73 · DOI: 10.1016/j.jelechem.2012.01.025

3 AUTHORS, INCLUDING:

Ann Laheäär
Skeleton Technologies
12 PUBLICATIONS **113** CITATIONS
SEE PROFILE

Alar Jänes
University of Tartu
109 PUBLICATIONS **1,817** CITATIONS
SEE PROFILE

Journal of Electroanalytical Chemistry 669 (2012) 67–72

Contents lists available at SciVerse ScienceDirect

Journal of Electroanalytical Chemistry

journal homepage: www.elsevier.com/locate/jelechem

Lithium bis(oxalato)borate as an electrolyte for micromesoporous carbide-derived carbon based supercapacitors

Ann Laheäär, Alar Jänes, Enn Lust *

Institute of Chemistry, University of Tartu, 14a Ravila Street, 50411 Tartu, Estonia

ARTICLE INFO

Article history:
Received 2 September 2011
Received in revised form 23 January 2012
Accepted 27 January 2012
Available online 8 February 2012

Keywords:
Supercapacitor
Carbide-derived carbon
LiBOB electrolyte
Carbonate solvents

ABSTRACT

1 M solution of lithium bis(oxalato)borate (LiBOB) in ethylene carbonate (EC) and dimethyl carbonate (DMC) mixture (1:1 volume ratio) was studied as an electrolyte for supercapacitors with high surface area micromesoporous carbide-derived carbon electrodes, synthesized from Mo_2C. Electrochemical characteristics were studied using cyclic voltammetry, electrochemical impedance spectroscopy (EIS) and constant current charge/discharge methods. The established region of ideal polarizability for a two-electrode system was ~3.0 V and the limiting capacitance, calculated from EIS data, was 125 F g^{-1}. Three-electrode measurements showed that solid electrolyte interface formation is a very complex process and partially blocks the adsorption and intercalation/deintercalation processes on the negatively charged electrode. The capacitance of a supercapacitor cell decreased by 33% during 5000 galvanic cycles between applied cell voltages from 1.5 V to 3.0 V. Calculated maximal energy and power densities were 42.5 W h kg^{-1} and 67.3 kW kg^{-1}, respectively. Thus, the tested LiBOB electrolyte is a potential candidate for long-lasting supercapacitors with high power density.

1. Introduction

The growing energy consumption in the world and increasing demand for energy storage devices for both portable and stationary applications drives the continuous development of supercapacitors (SC) [1–6] and lithium ion batteries (LIB) [7–10].

Lithium bis(oxalato)borate (LiBOB) has been studied before as an electrolyte salt (or additive) for LIBs [10–14]. Solid electrolyte interface (SEI) formation on interfaces between different electrode materials (graphite, lithium, nickel, etc.) and LiBOB based electrolytes has been discussed by several research groups [11–14]. However, to our knowledge, LiBOB has not been studied as an electrolyte salt for SC application. The aim of this paper was to establish the region of ideal polarizability, limiting capacitance, charge/discharge time constant, durability, and other electrochemical parameters, for a SC cell consisting of micromesoporous carbide-derived carbon (MMPC) electrodes and 1 M LiBOB electrolyte in a 1:1 volume mixture of ethylene carbonate (EC) and dimethyl carbonate (DMC).

2. Experimental

The tested electrodes comprised of 95 wt.% active material (carbon) and 5 wt.% binder (polytetrafluoroethylene 60% solution in H_2O (Aldrich)), rolled to form a ~105 ± 5 μm thick flexible layer of porous carbon with hierarchical structure [15–19]. The high-temperature chlorination method was used for synthesizing MMPC powder C(Mo_2C) from molybdenum carbide at 800 °C. Magnetron sputtering method was applied to deposit a thin Al layer on one side of the electrodes for good electrical contact and to reduce the ohmic potential drop for SC cell.

Nova 1200e (Quantachrome) system was used for nitrogen adsorption measurements, where Brunauer–Emmett–Teller (BET) method, non-local density functional theory and other models, discussed in detail in [15], were applied to study the porous carbon structure. The respective data are given in Table 1 and indicate that the electrode material is mainly microporous with some mesoporosity. More detailed C(Mo_2C) material characterization and pore size distribution data analysis can be found in [16].

Electrolyte was prepared from equimolecular mixture of very pure EC and DMC (Merck, Selectipur®) and dry LiBOB (Chemetall, standard battery grade). The solution was saturated with pure Ar (99.9999%) and all measurements were conducted in a glove box using hermetic two- and three-electrode standard cells (Hohsen Corp., Japan). Working electrodes (WE) and counter electrodes (CE) in three-electrode systems had cross-section surface areas of 0.28 cm^2 and 2.0 cm^2, respectively. Reference electrode (RE) was Li-ring (Li/Li^+) in the same electrolyte solution. Life time tests were conducted with two-electrode cell configurations, where the cross-section surface area was 2.0 cm^2 for both electrodes. Mesoporous polypropylene (Celgard® 2400) membranes were used. Electrodes

* Corresponding author. Tel.: +372 737 5165; fax: +372 737 5264.
E-mail address: enn.lust@ut.ee (E. Lust).

1572-6657/$ - see front matter © 2012 Elsevier B.V. All rights reserved.
doi:10.1016/j.jelechem.2012.01.025

Table 1
Gas phase characteristics of the C(Mo_2C) electrode material.

S_{BET} ($m^2\ g^{-1}$)	S_{micro} ($m^2\ g^{-1}$)	V_{micro} ($cm^3\ g^{-1}$)	V_{tot} ($cm^3\ g^{-1}$)
1675	1559	1.179	1.399

S_{BET} — BET multipoint surface area.
S_{micro} — *t-method* micropore area.
V_{micro} — *t-method* micropore volume.
V_{tot} — total pore volume.

were impregnated in the working electrolyte solution for 24 h before measurements.

Impedance spectra were recorded using a 1252A Solartron frequency response analyzer and a SI1287 potentiostat with a 5 mV modulation.

3. Electrochemical results and discussion

3.1. Cyclic voltammetry data

Cyclic voltammograms (CVs) for the three-electrode system were measured at potential scan rates v from 0.5 to 50 mV s^{-1} and in a wide WE potential E region from 0.5 to 5.0 V vs. Li/Li^+. CVs are presented as gravimetric capacitance C_g vs. WE potential E (vs. Li/Li^+) in Fig. 1a, calculated using Eq. (1):

$$C_g = \frac{jS_{el}}{vm}, \tag{1}$$

where j is current density, S_{el} is WE cross-section surface area, v is potential scan rate, and m is WE mass. Based on the measured data, the system does not reach equilibrium as C_g values depend on v in the whole region of applied v (Fig. 1a). The highest capacitance is obtained at high positive electrode potentials ($E > 4.5$ V), caused by the adsorption of BOB^- anions with partial charge transfer step [16–18]. At negative potential scan ($E < 1.0$ V), i.e. reduction curve, the formation of solid electrolyte interface (SEI) takes place [11–14,18,19]. The increase in capacitance during SEI formation is probably caused by the decrease in thickness of SEI or the increase in dielectric permittivity of the surface film. During the reverse potential scan (oxidation curve) the surface processes are very slow and blocked due to SEI, and thus low capacitance values have been obtained. Only at $E > 2.5$ V the oxidation of SEI-forming components seems to occur. The blocking effect of SEI seems to be the strongest for 1 M LiBOB + EC + DMC electrolyte, when compared to other Li-salts studied earlier – 1 M $LiPF_6$ and 1 M $LiClO_4$ in the same solvent mixture (Fig. 1b) [17]. The lowest gravimetric capacitance values were obtained for LiBOB electrolyte in the wide potential region studied, except near the switchover potentials (at both ends of the scanned potential region).

As can be seen from Fig. 1a and b, the cathodic cut-off potential (0.5 V) is by at least 0.5 V larger in relation to the point of zero charge potential (~3.0 V) than the corresponding anodic cut-off potential of 5.0 V. In addition to trivial effect of enlargement of the anodic current in the vicinity of the anodic cut-off potential due to oxidation of the intermediate species formed by reduction of electrolyte species close to the cathodic cut-off potential, there may exist a specific effect of trapping of cations in microporous carbons at excessively negatively charged carbon electrode surface [20]. Cations trapped in carbon micropores at extremely high electrode charge density cannot be desorbed in the native potential domain of the negatively charge carbon electrode, in other words partially irreversible adsorption/desorption occurs on the microporous surface of the studied electrodes.

The two-electrode test cell data showed that for C(Mo_2C)|1 M LiBOB + EC + DMC system nearly rectangular CVs can be obtained at cell voltages ΔV up to 3.0 V and at $v < 50$ mV s^{-1} (Fig. 2). Gravimetric capacitance C_g (per one electrode) was calculated using relation:

$$C_g = \frac{4C}{m_{el}}, \tag{2}$$

where C is the total capacitance of the test cell (F) and m_{el} is the mass of electrodes. The C_g values obtained are comparable to similar systems with 1 M $LiPF_6$ + EC + DMC [18] and 1 M $LiClO_4$ + EC + DMC [17] electrolytes. The increase in capacitance near $\Delta V > 2.9$ V is probably caused by the electroreduction of O_2 and H_2O traces at the negatively charged electrode, and oxidation of surface functionalities at the positively charged surface.

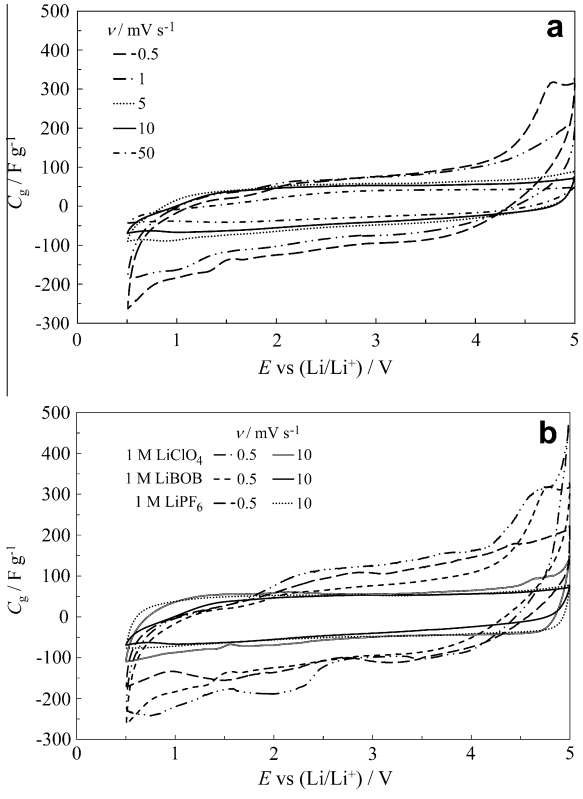

Fig. 1. Current density expressed as gravimetric capacitance vs. WE potential curves for (a) C(Mo_2C)|1 M LiBOB at different potential scan rates (noted in figure) and (b) different systems at 0.5 and 10 mV s^{-1}.

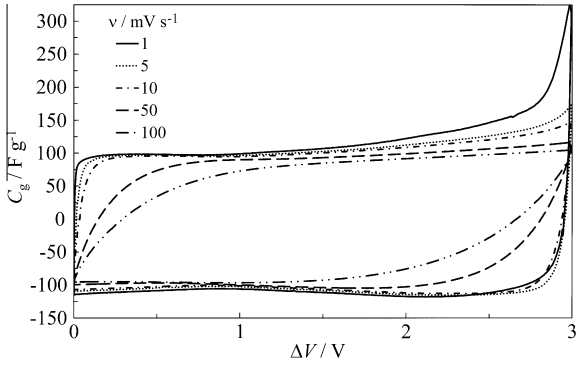

Fig. 2. Current density expressed as capacitance vs. cell voltage curves for two-electrode test cell at different potential scan rates.

3.2. Impedance spectroscopy data

Nyquist plots were measured for both two- and three-electrode systems in *ac* frequency range from 1×10^{-3} to 3×10^{5} Hz. The complex plane impedance plots obtained have three distinguishable regions (Figs. 3 and 4a). The slightly depressed semi-circle in high-frequency part ($1 \times 10^{3}...3 \times 10^{5}$ Hz) describes mixed kinetic processes (mainly charge transfer and adsorption) on the macroscopic surface of the porous carbon electrodes [17–19]. At middle frequencies (0.1–000 Hz) so-called 'porous electrode section' can be seen with the slope value of 45°, where the diffusion-like mass transfer process in the micromesopores of the MMPC electrodes is the rate-limiting process [17–19].

The shape of Z'',Z'-plots for the three-electrode C(Mo_2C)|1 M LiBOB + EC + DMC system (Fig. 3a) is very similar to the previously measured systems with other Li-salts [17]. According to the data, nearly capacitive behavior can be seen only at WE potentials from 1.5 to 4.0 V (vs. Li/Li^+), where the plots are almost vertical in the low-frequency region ($f < 0.1$ Hz). The limiting process in this region is adsorption of ions on/into the micromesoporous surface. At higher WE potentials ($E > 4.0$ V vs. Li/Li^+) adsorption of BOB^- anion with partial charge transfer occurs and the low-frequency behavior is no longer purely capacitive [21,22]. At lower WE potentials ($E \leqslant 1.5$ V vs. Li/Li^+) the adsorption/intercalation of Li^+ ions starts [21], described by mixed kinetic mechanisms. At ~1.0 V vs. Li/Li^+ SEI formation starts, which is a very complex mixed kinetic process.

The phase angle θ vs. log$f$ plots (Fig. 3b) indicate that noticeable deviation of LiBOB|MMPC interface from ideally polarizable adsorption step limited interface takes place at $E \geqslant 4.7$ V and $E \leqslant 1.5$ V. Thus, according to three-electrode system impedance data, the region of ideal polarizability for two-electrode system should be in the range of 3.0 V.

The impedance measurements of two-electrode systems affirm the conclusions of the earlier discussion as nearly ideal capacitive behavior has been established in the low-frequency region up to $\Delta V < 3.0$ V (Fig. 4). The macroheterogeneous charge transfer resistance R_m value (obtained according to the width of high-frequency semicircle) increases remarkably at $\Delta V \geqslant 3.0$ V, which is probably due to the beginning of the electroreduction of residual H_2O and O_2 traces and oxidation of various surface functional groups existing at micromesoporous carbon surface.

The limiting series capacitance C_s values calculated from Nyquist plots for two-electrode cell increase with increasing applied ΔV and reach almost 125 F g^{-1} in the low-frequency region at $\Delta V = 2.7$ V (Fig. 5), which is remarkably higher than in a similar system with 1 M $LiClO_4$ electrolyte [17] and practically the same as measured for 1 M $LiPF_6$ electrolyte in the same solvent mixture (the measured maximum value ~0.42 F cm^{-2} in the $LiPF_6$ system corresponds to ~125 F g^{-1}, when recalculated by using the mass of electrodes) [18]. However, at $\Delta V = 3.2$ V C_s is even higher than 129 F g^{-1}. The capacitance values calculated from Nyquist plots are in a good agreement with C_g values discussed above (CV data).

Characteristic charging/discharging time constants τ_R for two-electrode cells were calculated from the frequency of maxima f_{max} in imaginary capacitance C'' vs. log$f$ dependencies (Fig. 6) using relation:

$$\tau_R = \frac{1}{2\pi f_{max}}. \quad (3)$$

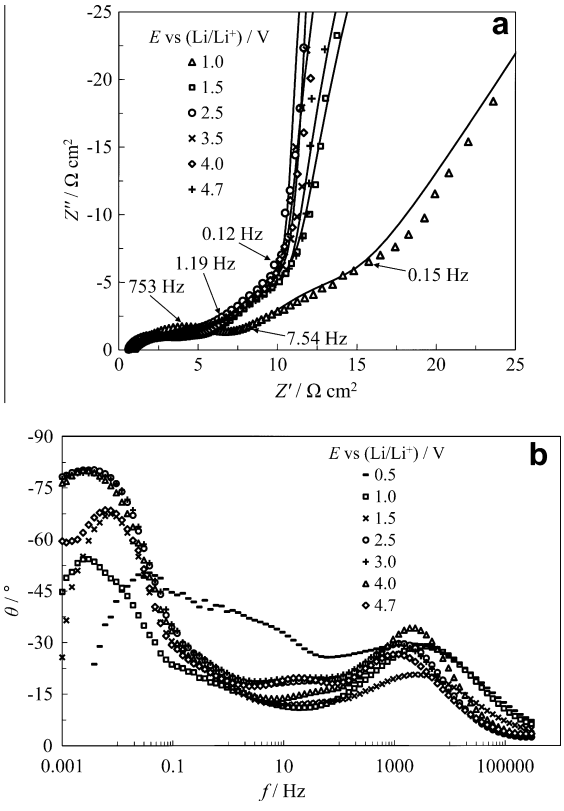

Fig. 3. Nyquist plots (points – experimental data, solid lines – fitting data using equivalent circuit in Fig. 7) (a) and phase angle vs. *ac* frequency (b) at different WE potentials for C(Mo_2C)|1 M LiBOB.

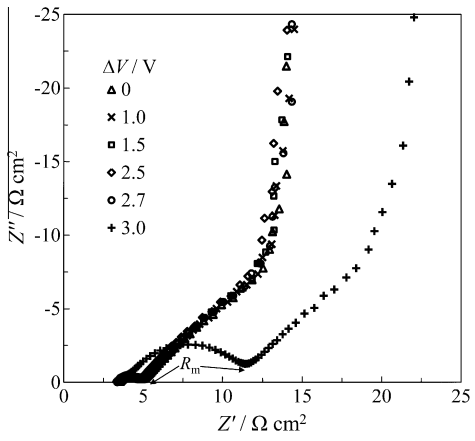

Fig. 4. Nyquist plots for two-electrode test cell at different cell voltages.

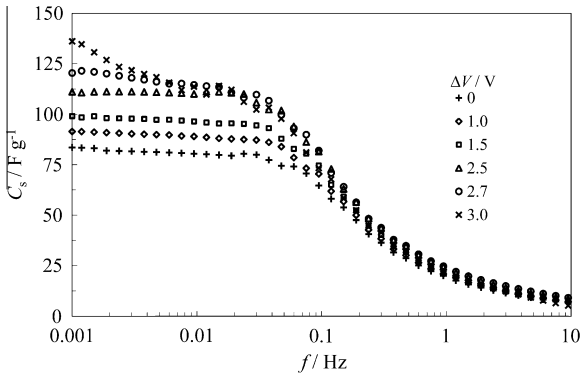

Fig. 5. Series capacitance vs. frequency plots for two-electrode test cell at different cell voltages.

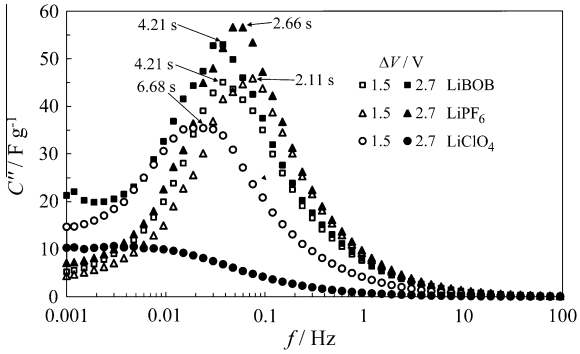

Fig. 6. Imaginary part of capacitance vs. frequency plots for two-electrode test cells based on LiBOB, $LiPF_6$ and $LiClO_4$ electrolytes at different cell voltages.

Comparison of LiBOB based system with data obtained for systems based on other Li-salts shows that time constant increases in the order of salts: $LiPF_6$ < LiBOB < $LiClO_4$. Time constant also depends on the voltage applied. For LiBOB based cell the time constant is 4.21 s at both 1.5 and 2.7 V, but it is shorter at ΔV < 1.5 V and increases at higher cell voltages.

The maximal energy density and power density values were calculated at ΔV = 3.0 V using relations [18,23–25]:

$$E_{max} = \frac{C_s S_{el} \Delta V^2}{2m3.6}. \quad (4)$$

$$P_{max} = \frac{\Delta V^2 S_{el}}{4R_s m}. \quad (5)$$

where C_s is low-frequency series capacitance, S_{el} is the cross-section surface area of electrodes (2 cm^2), ΔV is applied cell voltage, m is the mass of two electrodes, R_s is high-frequency series resistance (3.6 comes from conversion of time and mass units). Calculated E_{max} and P_{max} were 42.5 W h kg^{-1} and 67.3 kW kg^{-1}, respectively. However, it has to be noted that C_s includes a proportion of faradaic capacitance, so the obtained E_{max} value is probably somewhat overestimated.

3.3. Fitting of impedance data

The impedance complex plane plots of the three-electrode system were fitted using an equivalent circuit worked out by Meyers et al. (Fig. 7) [21]. In our previous study [17] the circuit was modified by adding a constant phase element CPE_2 into the low-frequency subcircuit to take into account the adsorption (electrical double layer formation) processes on/into the micromesoporous geometrically rough carbon surface at very low *ac* frequency

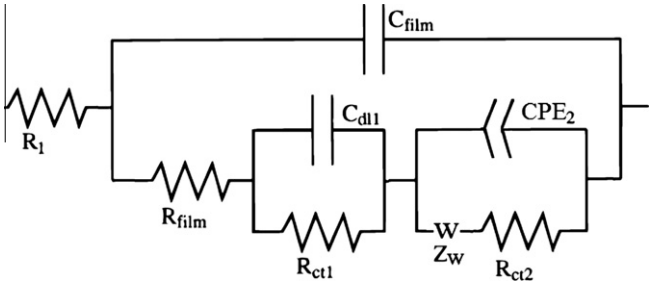

Fig. 7. Equivalent circuit used for fitting of impedance data (R_1 – high-frequency series resistance, C_{film} and R_{film} – surface film capacitance and resistance, R_{ct1} and C_{dl1} – external charge transfer resistance and capacitance, R_{ct2} and CPE_2 – internal charge transfer resistance and constant phase element, Z_w – Warburg-like diffusion impedance).

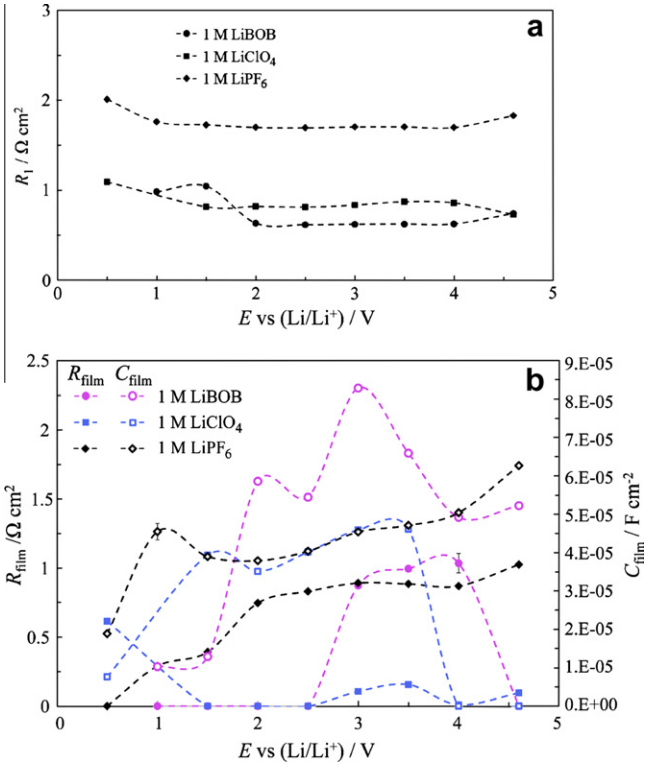

Fig. 8. High frequency series resistance (a), film resistance and capacitance (b) vs. working electrode potential dependencies for systems noted in figure.

(down to 0.001 Hz). R_{ct1} is related to faradaic charge transfer resistance at mesoporous surface areas and C_{dl1} is the respective capacitance. R_{ct2} is the faradaic charge transfer resistance value for microporous surface areas. A more detailed description and comments on the circuit choice can be seen in [17]. The good fitting of calculated data to experimental ones has been established (Fig. 3a) as the chi-square function for fitting was $\chi^2 \geqslant 6{\cdot}10^{-4}$ and $\Delta^2 \geqslant 9{\cdot}10^{-2}$. Models and equivalent circuits developed by Levi and Aurbach [26] for LIB multilayered porous composite electrodes and by Itagaki et al. for SCs (transmission line model) [27] were also tested, but the best fitting was achieved by applying the modified circuit described above.

The high-frequency series resistance R_1 (Fig. 8a) values are slightly lower compared to 1 M $LiClO_4$ system (~0.6 Ω cm^2) and increase a little at lower WE potentials due to the formation of SEI. Comparatively low surface film capacitance (C_{film}) and resistance (R_{film}) values have been observed (Fig. 8b), somewhat lower than those for other Li-salt based systems [17] at E < 1.5 V and E < 2.5 V, respectively. However, at $E \geqslant$ 3.0 V (vs. Li/Li^+) C_{film} and R_{film} are higher than for other Li-based systems tested [17], explained by very big molar volume of BOB^- anions.

The diffusion resistance (R_D) values (Fig. 9a) are noticeably higher than internal charge transfer resistance R_{ct2} (Fig. 9b), external charge transfer resistance R_{ct1} (not shown for shortness) and R_1 values in the LiBOB based system, similarly to other Li-salt based systems studied earlier [17]. BOB^- anion has larger dimensions compared to ClO_4^- or PF_6^- anions, therefore R_D values obtained are the highest for the system studied in this paper, but differently from earlier measurements, R_D values increase at lower WE potentials (E < 1.5 V vs. Li/Li^+). Fractional exponent α_w values (Fig. 9a) in diffusion impedance Eq. (6) are slightly higher than 0.5, indicating that the deviation of C(Mo_2C)|1 M LiBOB system from the classical semi-infinite diffusion model (α_w = 0.5) toward finite-length Warburg model with adsorption boundary condition [28–30] is surprisingly weak. Diffusion impedance Z_W is given as:

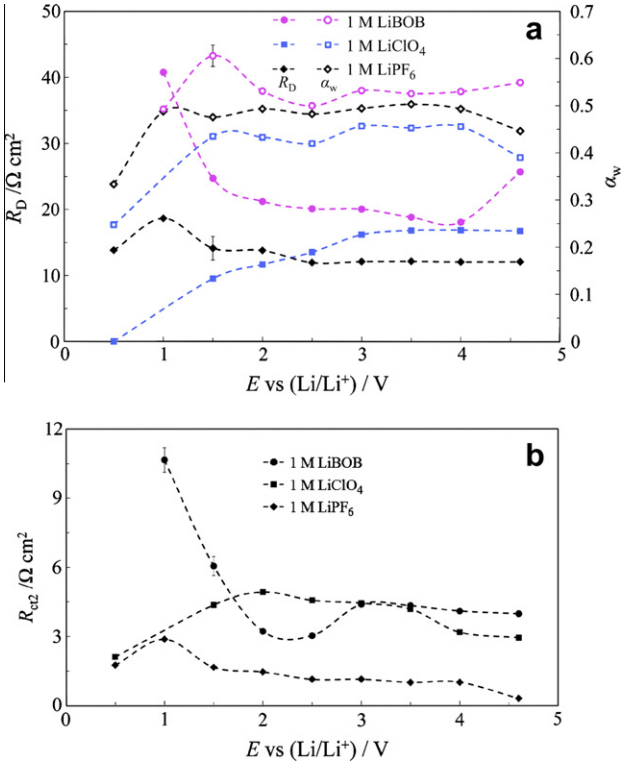

Fig. 9. Diffusion resistance and Warburg fractional exponent (a) and internal charge transfer resistance (b) vs. working electrode potential dependencies for systems noted in figure.

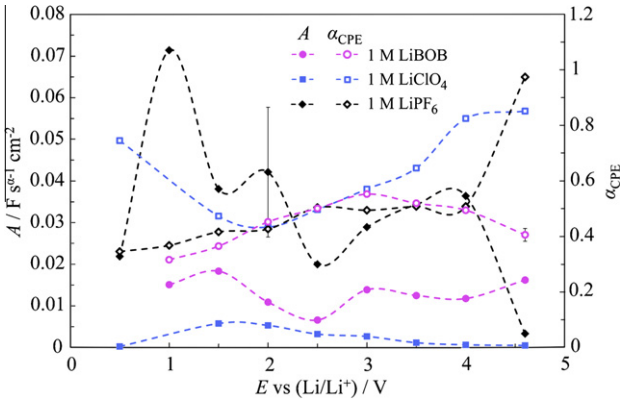

Fig. 10. Constant phase element (CPE) coefficient and CPE fractional exponent vs. working electrode potential dependencies for systems noted in figure.

$$Z_w = \sigma_{ads}(j\omega)^{-\alpha_w}. \quad (6)$$

where σ_{ads} is Warburg constant [31].

Low-frequency constant phase element impedance is expressed as:

$$Z_{CPE} = A^{-1}(j\omega)^{-\alpha_{CPE}}. \quad (7)$$

where A is CPE coefficient, ω is radial frequency, and α_{CPE} is fractional exponent (if $\alpha_{CPE} = 1.0$, then A = capacitance). Parameters A and α_{CPE} (Fig. 10) show that the deviation of C(Mo_2C)|1 M LiBOB interface from capacitive behavior is remarkable as $\alpha_{CPE} \sim 0.5$ has been established ($\alpha_{CPE} = 0.5$ is characteristic to semi-infinite diffusion process). The calculated moderate A values and $\alpha_{CPE} \sim 0.5$ for

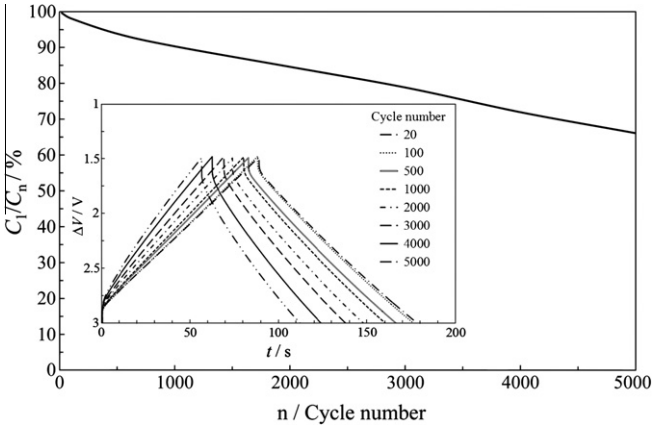

Fig. 11. Ratio of discharge capacitances of 1st and nth cycle vs. cycle number and galvanic cycles (figure inset) for two-electrode test cell at charging/discharging current density of 4 mA cm^{-2}.

C(Mo_2C)|1 M LiBOB interface show that LiBOB is not a very good candidate for high energy/power density SCs.

3.4. Time stability test

The life time of two-electrode systems was studied by constant current charging/discharging method. Five thousand galvanic cycles were measured at a current density of 4 mA cm^{-2} between 1.5 and 3.0 V (Fig. 11, inset). Capacitance values were calculated from the slopes of charge and discharge curves (C_C and C_D, respectively), where the linear part from 2.3 to 1.5 V has been used. The ratio C_D/C_C remained ~0.99 after 5000 cycles, which shows good energetic (i.e. Coulombic) efficiency of the system. However, the discharge capacitance value decreased by 33% from 1st cycle to 5000th cycle (Fig. 11) during time stability test. If the average applied cell voltage (from 0 to 2.2 V) and charging/discharging current density (1 mA cm^{-2}) were noticeably lower, then the capacitance retention was only 2.3% during 1000 cycles. Thus, the capacitance degradation is mainly caused by the faradaic processes starting to occur intensively at $\Delta V \geqslant 2.5$ V.

4. Conclusions

Two- and three-electrode supercapacitor test cells with micro-mesoporous carbide-derived carbon electrodes and 1 M LiBOB electrolyte in a solvent mixture of ethylene carbonate and dimethyl carbonate were completed and electrochemically characterized. Based on the data for three-electrode systems, 1 M LiBOB + EC + DMC electrolyte has the lowest gravimetric capacitance, compared to other Li-salt electrolytes studied earlier ($LiClO_4$ and $LiPF_6$) [17]. Impedance data showed that nearly ideal capacitive behavior is obtained only at working electrode potentials from 1.5 to 4.0 V (vs. Li/Li^+). The formation of SEI is a very complex process taking place at $E < 1.0$ V (vs. Li/Li^+), which causes the partial blocking of the micromesoporous electrode surface.

Experimental Nyquist (Z'',Z') plots were fitted with data calculated by using a modified equivalent circuit [17], originally worked out by Meyers et al. [21]. The resistance values obtained (internal and external charge transfer, film and diffusion resistances) for the LiBOB based system are comparable or somewhat higher than those for other Li-salts. Diffusion resistance values are very high due to the much larger dimensions of BOB^- anion.

The region of ideal polarizability for the two-electrode test cell was ~3.0 V. Limiting capacitance was up to 125 F g^{-1} and calculated time constant values were shorter than for similar systems with $LiClO_4$ electrolyte, but longer than for $LiPF_6$ based test cell. Although

quite high maximal energy and power densities were calculated (42.5 W h kg^{-1} and 67.3 kW kg^{-1}, respectively, the capacitance decreased by 33% during 5000 charge/discharge cycles between 1.5 V and 3.0 V. Thus, 1 M LiBOB electrolyte with carbonate solvents is not a very desirable choice for long-lasting high energy and power density supercapacitors.

Acknowledgements

This work has been partially supported by Estonian Science Foundation Grant No. 8172, Estonian Ministry of Education and Research (Project SF0180002s08), European Regional Development Fund Project SLOKT10209T, and by graduate school 'Functional materials and processes' receiving funding from the European Social Fund under Project 1.2.0401.09-0079 in Estonia.

Authors thank Chemetall GmbH for providing LiBOB salt.

References

[1] B.E. Conway, Electrochemical Supercapacitors: Scientific Fundamentals and Technological Applications, Kluwer Academic/Plenum Publishers, New York, 1999.
[2] E. Frackowiak, F. Béguin, Carbon 39 (2001) 937.
[3] P. Simon, Y. Gogotsi, Nat. Mater. 7 (2008) 845.
[4] T. Thomberg, A. Jänes, E. Lust, J. Electroanal. Chem. 630 (2009) 55.
[5] P.L. Taberna, P. Simon, J.F. Fauvargue, J. Electrochem. Soc. 150 (2003) A292.
[6] E. Lust, A. Jänes, M. Arulepp, J. Solid State Electrochem. 8 (2004) 488.
[7] G.-A. Nazri, G. Pistoia (Eds.), Lithium Batteries: Science and Technology, Kluwer Academic Publishers, New York, 2004.
[8] D. Aurbach, in: D. Aurbach, D. Orbakh (Eds.), Nonaqueous Electrochemistry, Marcel Dekker, New York, 1999. (Chapters 1, 4, 6).
[9] E. Peled, in: J.P. Gabano (Ed.), Lithium Batteries, Oxford University Press, London, 1983. (Chapter 3).
[10] R. Marom, O. Haik, D. Aurbach, I.C. Halalay, J. Electrochem. Soc. 157 (2010) A972.
[11] K. Xu, S.S. Zhang, U. Lee, J.L. Allen, T.R. Jow, J. Power Sources 146 (2005) 79.
[12] L. Yang, M.M. Furczon, A. Xiao, B.L. Lucht, Z. Zhang, D.P. Abraham, J. Power Sources 195 (2010) 1698.
[13] L. Larush-Asraf, M. Biton, H. Teller, E. Zinigrad, D. Aurbach, J. Power Sources 174 (2007) 400.
[14] J.-C. Panitz, U. Wietelmann, M. Wachtler, S. Ströbele, M. Wohlfahrt-Mehrens, J. Power Sources 153 (2006) 396.
[15] S.J. Gregg, K.S.W. Sing, Adsorption Surface Area and Porosity, Academic Press, London, 1982.
[16] A. Jänes, T. Thomberg, H. Kurig, E. Lust, Carbon 47 (2009) 23.
[17] A. Laheäär, A. Jänes, E. Lust, Electrochim. Acta 56 (2011) 9048.
[18] A. Laheäär, H. Kurig, A. Jänes, E. Lust, Electrochim. Acta 54 (2009) 4587.
[19] M. Eikerling, A.A. Kornyshev, E. Lust, J. Electrochem. Soc. 152 (2005) E24.
[20] D. Aurbach, M.D. Levi, G. Salitra, N. Levy, E. Pollak, J. Muthu, J. Electrochem. Soc. 155 (2008) A745.
[21] J.P. Meyers, M. Doyle, R.M. Darling, J. Newman, J. Electrochem. Soc. 147 (2000) 2930.
[22] E. Barsoukov, J.R. Macdonald (Eds.), Impedance Spectroscopy Theory Experiment and Applications, Wiley Interscience John Wiley & Sons, New Jersey, 2005.
[23] M. Arulepp, J. Leis, M. Lätt, F. Miller, K. Rumma, E. Lust, A.F. Burke, J. Power Sources 162 (2006) 1460.
[24] M. Arulepp, L. Permann, J. Leis, A. Perkson, K. Rumma, A. Jänes, E. Lust, J. Power Sources 133 (2004) 320.
[25] A.F. Burke, J. Power Sources 91 (2000) 37.
[26] M.D. Levi, D. Aurbach, J. Phys. Chem. B 108 (2004) 11693.
[27] M. Itagaki, S. Suzuki, I. Shitanda, K. Watanabe, H. Nakazawa, J. Power Sources 164 (2007) 415.
[28] T. Jacobsen, K. West, Electrochim. Acta 40 (1995) 233.
[29] A. Compte, Phys. Rev. E 53 (1996) 4191.
[30] J. Bisquert, G. Garcia-Belmonte, P. Bueno, E. Longo, L.O.S. Bulhões, J. Electroanal. Chem. 452 (1998) 229.
[31] ZView for Windows (version 2.8d), Scribner Associates, Inc., NC.